DOI: 10.1021/ma101726v

Macromolecules
ARTICLE

Control of Nanophases in Polyelectrolyte Gels by Salt Addition

Kuo-An Wu,[†] Prateek K. Jha,[‡] and Monica Olvera de la Cruz*[,†,‡,§]

[†]*Department of Materials Science and Engineering, Northwestern University, Evanston, Illinois 60201, United States,* [‡]*Department of Chemical and Biological Engineering, Northwestern University, Evanston, Illinois 60201, United States, and* [§]*Department of Chemistry, Northwestern University, Evanston, Illinois 60201, United States*

Received July 29, 2010; Revised Manuscript Received September 16, 2010

ABSTRACT: We propose a continuum theory to describe the influence of salt on the phase segregation behavior of polyelectrolyte gels. The equilibrium phase behavior is determined by the steady state solution of time-dependent Ginzburg−Landau evolution equations using an efficient spectral technique. Numerical solutions of a model system with density inhomogeneities in one direction show a transition between no phase separation (swollen gel), nanophase segregation (lamellar nanostructures), and macrophase separation (collapsed gel); as the salt concentration increases. The wavelength of nanophases increases with the salt concentration and the resulting parameter regime of nanophases depends strongly on the salt concentration. We augment the numerical solutions with a weakly nonlinear analysis, that describes primary consequences of salt addition and highlights the effect of nonlinearities on the phase segregation behavior.

Introduction

Polyelectrolyte (PE) gels are becoming strong candidate materials for in vivo drug carriers, artificial muscles, and microfluidic devices; besides their current use in disposable diapers and sanitary napkins.[1−6] They possess a rich phase behavior originating from the intricate balance of network elasticity, van der Waals forces, and electrostatic interactions that can be tuned by environmental stimuli such as temperature, pH, salt, light, electric field, etc.[7−12] This includes their ability to undergo large reversible volume changes with increase in solvent hydrophilicity or an increase in charge of the polymer backbone. In situations where the electrostatic and the van der Waals forces between the monomers compete, that is, for PE gels in poor solvents, an intranetwork phase separation occurs—to regions dense and depleted in polymer.[13−17] The intranetwork phase separation in PE gels is conceptually similar to the microphase separation of polyelectrolyte solutions, but is more pronounced in gels as the elastic retractions of the network structure pose restrictions to a complete collapse. Moreover, the size of the resulting dense domains are often in the nanometer range,[18,19] and are dictated by the network inhomogeneities and thermal fluctuations.[20−22] The coexistence of dense ionic regions with dilute swollen regions opens possibility for their use as porous nanochannels for microfluidic transport and similar applications.

Classical descriptions of polyelectrolyte gels were derived using the Flory−Huggins theory of polymer solutions and the classical theory of rubber elasticity.[23−25] Electrostatic effects enter these descriptions as the translational entropy of mobile ions determined by an analogy with the Donnan membrane potential[26] of the association−dissociation equilibria of the salt in the gel and in the solvent bath. The Coulomb interactions are neglected assuming the gel to be homogeneous and therefore electrically neutral. However, the assumption of homogeneity is no longer valid at nanometer length scales where nanophase segregation is expected, and more refined theories are needed to capture the phase behavior.[27−29] Recently, Jha et al.[30] have developed a model of salt-free gels with one-dimensional density inhomogeneities, where the Coulomb interactions are handled by the full solution of Poisson equation using a Green's function formalism. A numerical free energy minimization was carried out using the gradient projection algorithm to establish the inception criterion and the domain size of the resulting lamellar nanostructures. Comparing these results with those obtained from a linear model based on the random phase approximation (RPA), they showed the importance of nonlinear effects in the study of nanophases in gels.

In this paper, we propose a continuum theory of polyelectrolyte gels to investigate the salt effects on their nanophase segregation behavior. The free energy functional of Jha et al. is extended to include salt effects, and equilibrium phase behavior is determined by the steady state solution of time-dependent Ginzburg−Landau evolution equations using an efficient spectral technique.[31] The numerical solutions show a transition between no phase separation, nanophase segregation, and macrophase separation. The parameter regime and the wavelength of the nanophase show strong dependence on the salt concentration. We also present a weakly nonlinear analysis that provides useful insight into the underlying physics of this phase segregation behavior, and shows reasonable agreement with the numerical solutions.

Model

A proper thermodynamic description of polyelectrolyte gels requires the knowledge of various forces that influence their response for the length and time scales in consideration. At macroscopic length scales of homogeneous networks, gel response is determined by the solvent-mediated van der Waals forces between monomers, the translational entropy of mobile ions, and the elastic restoring forces of the network. Assuming that the degrees of freedom associated with all these interactions are independent of each other, a normalized free energy density of a gel sample of volume V can be given as the sum of individual

*E-mail: m-olvera@northwestern.edu.

 Published on Web 10/04/2010

interactions,

$$\overline{F} = \frac{F_t a^3}{k_B T V} = \overline{F}_{vdW} + \overline{F}_{entropic} + \overline{F}_{elastic} \quad (1)$$

where F_t is the total free energy, a is the monomer size taken equal to that of solvent molecules and mobile ions, k_B is the Boltzmann constant, and T is the temperature. The van der Waals interactions, $\overline{F}_{vdW}$, is given by,

$$\overline{F}_{vdW} = \chi\bar{\phi}(1-\bar{\phi}) + (1-\bar{\phi})\ln(1-\bar{\phi}) \quad (2)$$

where χ is the Flory−Huggins parameter for solvent quality, and $\bar{\phi}$ is the volume fraction of the monomers. Second term in eq 2 can be interpreted as the mixing contribution or the entropy of solvent molecules. The translational entropy of mobile ions gives rise to a contribution,

$$\overline{F}_{entropic} = \bar{c}\ln\bar{c} + \bar{s}\ln\bar{s} \quad (3)$$

where $\bar{c}$ and $\bar{s}$ are the volume fractions of the co-ions and counterions, respectively. The linear terms are neglected here due to the conserved ion and polymer constraints discussed below. For a salt volume fraction c_s and a monomer charge fraction f, $\bar{c} = c_s$, and $\bar{s} = c_s + f\bar{\phi}$, where the polymer is assumed to be negatively charged and all ions are monovalent. We assume the gel to be strongly charged and at constant pH, such that the monomer charge fraction (or the fraction of ionized groups) can be treated as constant. The elasticity of the network is obtained under the assumption of affine deformation of a network of cubic topology, composed of finite strands of N monomers between the cross-links. Since charged chains have the tendency of being overstretched, we use the inverse Langevin approximation to describe chain elasticity. That is, the net force acting on a chain is given by the inverse Langevin function, $\mathcal{L}^{-1}(H) \approx (3H - H^3)/(1 - H^2)$,[32,30] where H is the scaled extension defined as the ratio of the end-to-end distance of the chain (h) to the maximum possible extension ($h_{max} = Na$). The elastic free energy density is given by the integral of $\mathcal{L}^{-1}(H)$ multiplied by the density of strands, which reads after simplification,

$$\overline{F}_{elastic} = \frac{\bar{\phi}}{3}\left\{\frac{3\zeta}{4} - \ln\left[1 - \frac{3\zeta}{2}\right]\right\} \quad (4)$$

where $\zeta = 2/(3^{1/3}N^{4/3}\bar{\phi}^{2/3})$, assuming isotropic deformation.

Combining eqs 2, 3, and 4, the free energy density of the homogeneous gel (eq 1) is given as,

$$\overline{F} = \chi\bar{\phi}(1-\bar{\phi}) + (1-\bar{\phi})\ln(1-\bar{\phi}) + \bar{c}\ln\bar{c} + \bar{s}\ln\bar{s} + \frac{\bar{\phi}}{3}\left\{\frac{3\zeta}{4} - \ln\left[1 - \frac{3\zeta}{2}\right]\right\} \quad (5)$$

Extension of the above formalism to an inhomogeneously deformed gel requires replacing the average volume fractions, $\{\bar{\phi}, \bar{c}, \bar{s}\}$, by the local volume fractions, $\{\phi(\vec{r}), c(\vec{r}), s(\vec{r})\}$, followed by an integration over the gel volume. Inhomogeneities also give rise to an additional interfacial energy, $C|\nabla\phi|^2$, where $C = 1/36\bar{\phi}(1 - \bar{\phi})$ is a coefficient derived using the random phase approximation of polymer solutions.[24] Further, a Coulomb term needs to be included to account for the excess charge, $\rho(\vec{r}) = s(\vec{r}) - c(\vec{r}) - f\phi(\vec{r})$, that builds up in the gel in the event of nanophase segregation. In the following

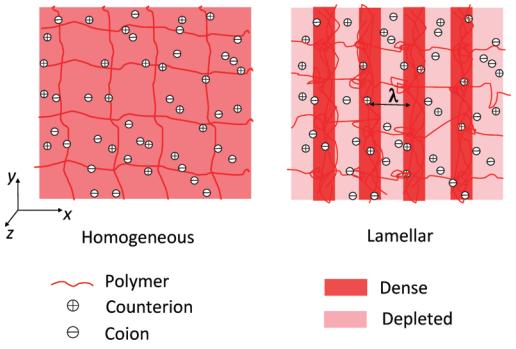

Figure 1. Homogeneous (swollen) and lamellar phases of the model polyelectrolyte gel.

discussion, the spatial dependence of volume fractions is assumed to be implicit for brevity, meaning $\{\phi, c, s, \rho\} \equiv \{\phi(\vec{r}), c(\vec{r}), s(\vec{r}), \rho(\vec{r})\}$. The free energy functional for the inhomogeneous gel is given by

$$F = \int d\vec{r}\left\{\frac{\xi}{6}\times\frac{\phi}{2}(\mu_1^2 + \mu_2^2 + \mu_3^2) - \frac{\phi}{3}\ln\left[1 - \frac{\xi}{2}(\mu_1^2 + \mu_2^2 + \mu_3^2)\right]\right\} + \int d\vec{r}\ \{\chi\phi(1-\phi) + (1-\phi)\ln(1-\phi) + c\ln c + s\ln s + C|\nabla\phi|^2\} + \int d\vec{r}\left\{\rho\Phi - \frac{1}{8\pi l_B}|\nabla\Phi|^2\right\} \quad (6)$$

in dimensionless units with a and k_BT being the length and energy scales respectively, and the above integral is over the volume of the inhomogeneous gel. $\Phi \equiv \Phi(\vec{r})$ is the dimensionless electrostatic potential obtained as the solution of the Poisson equation $\nabla^2\Phi = -4\pi l_B\rho$, where $l_B = e^2/4\pi\varepsilon\varepsilon_0 k_B T a$ is the dimensionless Bjerrum length; ε and ε_0 being the relative static permittivity of the solvent and the vacuum permittivity, respectively. The first two terms in eq 6 are the elastic energy of the polymer network subjected to a general deformation with eigenvalues μ_1, μ_2, and μ_3 derived using the inverse Langevin approximation discussed above. These eigenvalues are related to changes in the polymer volume fraction by $\mu_1\mu_2\mu_3 = \bar{\phi}/\phi$.

To illustrate salt effects on the nanophase segregation behavior of gels, we consider a simplified model with inhomogeneities only in the x-direction, that is, $\mu_2 = \mu_3 = 1$ and $\mu_1 = \bar{\phi}/\phi$. In this picture, the nanophase will correspond to lamellar domains of periodicity λ as shown in Figure 1. Equation 6 reduces to

$$F = \int d\vec{r}\left\{\frac{\xi}{6}\times\frac{\phi}{2}\left[2 + \left(\frac{\bar{\phi}}{\phi}\right)^2\right] - \frac{\phi}{3}\ln\left(1 - \frac{\xi}{2}\left[2 + \left(\frac{\bar{\phi}}{\phi}\right)^2\right]\right) + \chi\phi(1-\phi) + (1-\phi)\ln(1-\phi) + C|\nabla\phi|^2 + c\ln c + s\ln s + \left[\rho\Phi - \frac{1}{8\pi l_B}|\nabla\Phi|^2\right]\right\} \quad (7)$$

The equilibrium density distributions $\{\phi, c, s\}$ and the electrostatic potential Φ are determined by the minimization of the free energy functional (eq 7). The minimization procedure is carried out under the conservation constraints,

$$\int d\vec{r}\ [\phi - \bar{\phi}] = 0, \int d\vec{r}\ [c - \bar{c}] = 0, \int d\vec{r}\ [s - \bar{s}] = 0 \quad (8)$$

where $(\bar{\phi}, \bar{c}, \bar{s})$ are the average volume fractions. Note that the electroneutrality condition

$$\int \mathrm{d}\vec{r}\ [s - c - f\phi] = 0 \tag{9}$$

is automatically satisfied.

Numerical Solutions

The equilibrium phase behavior is attained by the steady-state solution of the time-dependent Ginzburg−Landau equations

$$\frac{\partial X_i}{\partial t} = -\Gamma_{X_i}\frac{\delta F}{\delta X_i} \tag{10}$$

where X_i represent $\{\phi, c, s, \Phi\}$ and Γ_{X_i} are phenomenological constants. The system evolves toward the free energy minimum through these dynamical equations since

$$\frac{\mathrm{d}F}{\mathrm{d}t} = \int \mathrm{d}\vec{r} \sum_{X_i}\frac{\delta F}{\delta X_i}\frac{\partial X_i}{\partial t} = \int \mathrm{d}\vec{r}\left[-\sum_{X_i}\Gamma_{X_i}\left(\frac{\delta F}{\delta X_i}\right)^2\right] < 0 \tag{11}$$

Thus, the volume fraction distributions $\{\phi, c, s\}$ and the electrostatic potential Φ that minimize eq 7 are obtained when the dynamic equations reach steady state (i.e., $\partial\phi/\partial t = 0$, $\partial c/\partial t = 0$, $\partial s/\partial t = 0$, and $\partial\Phi/\partial t = 0$).

Equation 10 with the usage of the free energy functional F (eq 7) does not meet the conservation constraints listed in eq 8. Thus, we use a modified free energy functional

$$F' = F + \Lambda_\phi \int \mathrm{d}\vec{r}\ [\phi(\vec{r}) - \bar{\phi}] + \Lambda_c \int \mathrm{d}\vec{r}\ [c(\vec{r}) - \bar{c}] + \Lambda_s \int \mathrm{d}\vec{r}\ [s(\vec{r}) - \bar{s}] \tag{12}$$

with the Lagrange multipliers

$$\Lambda_{X_i} = -\frac{\int \mathrm{d}\vec{r}\ \dfrac{\delta F}{\delta X_i}}{\int \mathrm{d}\vec{r}} \tag{13}$$

The modified evolution equations that obey the conservation constraints listed in eq 8 are

$$\frac{\partial X_i}{\partial t} = -\Gamma_{X_i}\frac{\delta F'}{\delta X_i} \tag{14}$$

Note that the values of Lagrange multipliers, Λ_{X_i}, change as $\{\phi,c,s\}$ evolve toward the free energy minimum state through above equations. Hence, Λ_{X_i} are updated using eq 13 for each iteration.

Since the electrostatic fields reach equilibrium much faster than redistribution of volume fractions, the electrostatic potential can be treated as in equilibrium state at any instant (i.e., $\partial\Phi/\partial t = 0$) on the time scales of volume fraction redistribution. Therefore, the evolution equation of Φ becomes

$$\frac{\partial\Phi}{\partial t} = -\Gamma_\Phi\frac{\delta F'}{\delta\Phi} = 0 = -\Gamma_\Phi\left[\rho + \frac{1}{4\pi l_B}\nabla^2\Phi\right] \tag{15}$$

which recovers the Poisson equation, $\nabla^2\Phi = -4\pi l_B\rho$.

The numerical solution of the evolution equations (eq 14) is complicated by the nonlinearities in the free energy functional (eq 7). Making use of the periodic symmetry inherent in our model, we employ periodic boundary conditions, and the evolution equations are solved using an efficient spectral technique.[31] Although our numerical scheme is conceptually similar to the gradient projection algorithm used by Jha et al.,[30] it has several advantages over the former approach. First, for a smoothly varying lamellar solution, the spectral method requires lesser number of grid points to resolve the same numerical accuracy. Second, compared to the real space Green's function solution for Φ used by Jha et al.,[30] the solution of Poisson equation in the reciprocal space is simpler

$$\Phi_{\vec{K}} = 4\pi l_B\frac{\rho_{\vec{K}}}{|\vec{K}|^2} \tag{16}$$

where $\Phi_{\vec{K}}$ and $\rho_{\vec{K}}$ are the Fourier amplitudes associated with Φ and ρ respectively. Φ is associated with $\{\rho_{\vec{K}}\}$ through the relation,

$$\Phi = \sum_{\vec{K}}\Phi_{\vec{K}}e^{i\vec{K}\cdot\vec{r}} = 4\pi l_B\sum_{\vec{K}}\frac{\rho_{\vec{K}}}{|\vec{K}|^2}e^{i\vec{K}\cdot\vec{r}} \tag{17}$$

Third, the evolution equations provide a general framework to study dynamics in these systems, if proper mobility coefficients are inserted for the phenomenological constants Γ_{X_i} in eq 14 and diffusion dynamics is introduced for corresponding physical quantities. However, since the equilibrium solutions do not depend on Γ_{X_i}, we set them equal to unity in this work.

To explore the parameter regime for nanophase segregation, we solve the evolution equations for different box length L_x along x-direction. The periodicity of the minimum energy density state, λ, is determined from the steady state profiles. The wavelength of lamellar phase is characterized by a finite nonzero λ, while a homogeneous solution and an unbounded energy density solution correspond to no phase separation and macrophase separation, respectively. The numerical solution is carried out with a mesh size Δx less than $\pi/4$ (in units of a) to ensure numerical accuracy. A time step Δt between 0.001−0.01 is used, in dimensionless units.

The excess free energy density, ΔF, defined as the energy difference between the steady state solution and the swollen gel (i.e., eq 5) per unit volume, is plotted as a function of L_x for various salt concentrations in Figure 2 and 3 for $(\bar{\phi}, \chi, f, l_B) = (0.05, 2.4, 0.5, 1.0)$. For the salt-free case in Figure 2, the swollen gel is stable against perturbations. The nanophase starts to appear as a small amount of salt is added into the system. In the region where the lamellar phase is the ground state, the wavelength of the lamellar phase increases with salt concentration. This trend continues until the salt concentration exceeds a critical value, in this case, $c_s \sim 1 \times 10^{-2}$, beyond which minimum energy density state is that corresponding to $L_x \to \infty$, meaning macrophase separation, as illustrated in Figure 3. Multiple free energy minima are observed as L_x increases continuously, as shown in Figure 2. However, the nanophases observed at higher values of L_x are exactly the same lamellar nanophase that appears at the first free energy density minimum but with multiple periods. For the above parameters, we find that

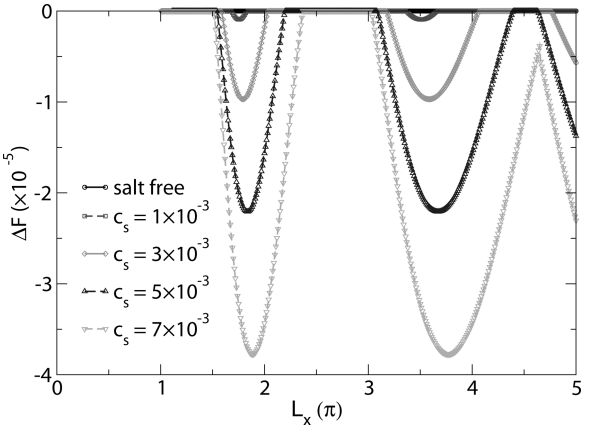

Figure 2. Excess free energy density ΔF against system length L_x in x-direction, showing the swollen gel−nanophase transition with increase in salt concentration. The model parameters are $\bar{\phi} = 0.05$, $N = 100$, $\chi = 2.4$, $f = 0.5$, and $l_B = 1$. For $L_x < 1$, the swollen gel state is the ground state.

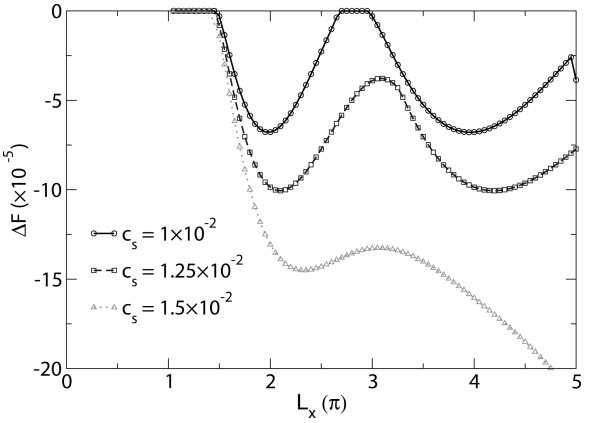

Figure 3. Excess free energy density ΔF against system length L_x in x-direction, showing the nanophase−macrophase transition with increase in salt concentration. The model parameters are $\bar{\phi} = 0.05$, $N = 100$, $\chi = 2.4$, $f = 0.5$, and $l_B = 1$. For $L_x < 1$, the swollen gel state is the ground state.

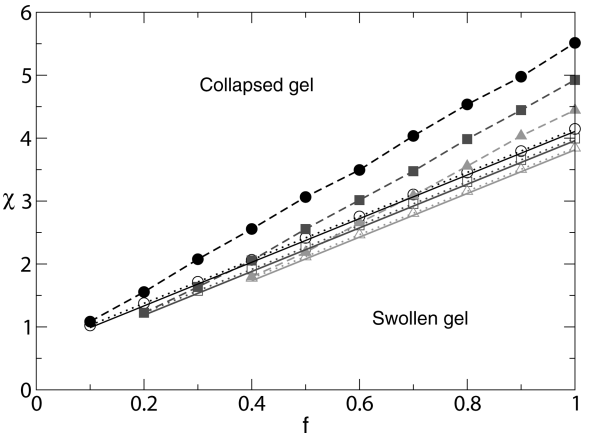

Figure 4. $\chi-f$ phase diagram for different salt concentrations. Swollen gel − nanophase transition lines are shown in dotted (hollow symbols) and solid lines for numerical solutions and weakly nonlinear analysis. The nanophase−macrophase transition lines computed from numerical solutions are represented by dashed lines (filled symbols). Salt-free, $c_s = 1 \times 10^{-2}$, and $c_s = 2 \times 10^{-2}$ are represented by circles, squares, and triangles, respectively. The model parameters are $\bar{\phi} = 0.05$, $N = 100$, and $l_B = 1$.

the wavelength of the lamellar nanophase increases by ∼12% as the salt concentration varies from 0.001 to 0.01. As is evident, inhomogeneities can be induced by the introduction of salt, that suggests salt addition as a promising means to control the nanophase segregation behavior.

To examine the influence of salt on the phase behavior in more detail, we construct phase diagrams as shown in Figure 4 and Figure 5. In Figure 4, we plot the $\chi-f$ phase diagram for a fixed Bjerrum length ($l_B = 1.0$) and various salt concentrations. For each value of f, the inception of nanophase from swollen phase is determined by increasing χ from a very low value (good solvent regime) in small steps until the inhomogeneities start to develop. The onset of macrophase separation from nanophase regime is obtained by running an extended system in x-direction (i.e., $L_x = 8\pi$) and keep increasing χ until the gel collapses. The shift of the nanophase−macrophase is observed to be larger than the swollen gel−nanophase phase boundary as the salt concentration increases. This translates to significant shrinkage of the stable nanophase region with increase in salt concentration. For much higher salt concentrations, the region of stable nanophase eventually collapses. In Figure 5, the $f-c_s$ phase diagram is plotted for a fixed value of χ and various Bjerrum lengths. The phase boundaries are determined in a similar fashion as stated earlier.

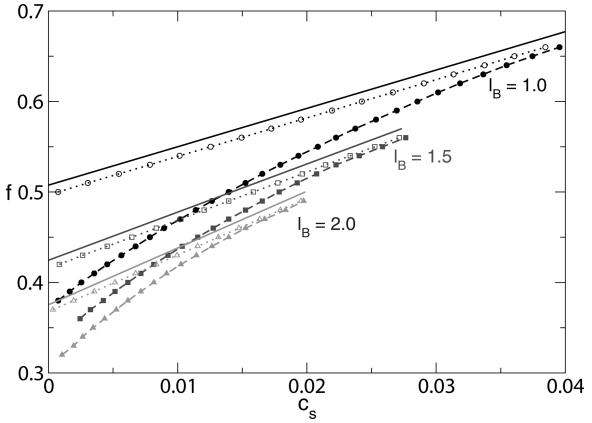

Figure 5. $f-c_s$ phase diagram for different Bjerrum length. Swollen gel−nanophase transition lines are shown in dotted (hollow symbols) and solid lines for numerical solutions and weakly nonlinear analysis. The nanophase−macrophase transition lines computed from numerical solutions are represented by dashed lines (filled symbols). The model parameters are $\bar{\phi} = 0.05$, $N = 100$, and $\chi = 2.40$.

In summary, it is suggested that nanophases are relatively easier to form in a polyelectrolyte gel in solvents with high dielectric permittivity and/or low salt concentrations.

An intuitive way to understand these phase diagrams is to re-examine how salt enters into the free energy functional in eq 7. On the one hand, salt ions lead to an additional translational entropy compared to the salt-free case. Hence, any localization of the monomers driven by the hydrophobic interactions, quantified by the interfacial energy coefficient C and the solvent quality χ, competes with the tendency of the mobile ions to be more dispersed because of the higher entropy; giving rise to an early inception of nanophases in certain cases as seen in Figure 2. On the other hand, screening by salt or an increase in dielectric permittivity of solvent reduces the Coulomb repulsions, giving rise to a shrinkage of nanophase region as seen in Figure 4 and Figure 5. In fact, for very high salt concentration or very low dielectric permittivity of solvent, we expect the gel to undergo a continuous transition from swollen to collapse phase with no intermediate nanophases. It is important to point out that the various physical interactions in our model system are strongly coupled to each other and are highly nonlinear. Therefore, the above reasoning based on pure intuition, is insufficient to describe the entire phase diagram. To analyze the nonlinear effects in more detail, and to gain further insight into the phase behavior, we perform a weakly nonlinear analysis discussed in the following section.

Weakly Nonlinear Analysis

For small perturbations in volume fractions from the homogeneous phase, the free energy functional of the model gel can be approximated by a Taylor expansion to the fourth order around the homogeneous solutions,

$$\mathcal{F} = \int \mathrm{d}\vec{r}\; g(\phi, c, s) + C|\nabla\phi|^2 + \left[\rho\Phi - \frac{1}{8\pi l_B}|\nabla\Phi|^2\right]$$

$$\simeq \int \mathrm{d}\vec{r}\; g(\bar{\phi}, \bar{c}, \bar{s}) + \frac{1}{2}\frac{\partial^2 g}{\partial\phi^2}\bigg|_{\bar{\phi},\bar{c},\bar{s}} \delta\phi^2 + \frac{1}{2}\frac{\partial^2 g}{\partial c^2}\bigg|_{\bar{\phi},\bar{c},\bar{s}} \delta c^2 + \frac{1}{2}\frac{\partial^2 g}{\partial s^2}\bigg|_{\bar{\phi},\bar{c},\bar{s}} \delta s^2$$

$$+ \frac{1}{4!}\frac{\partial^4 g}{\partial\phi^4}\bigg|_{\bar{\phi},\bar{c},\bar{s}} \delta\phi^4 + \frac{1}{4!}\frac{\partial^4 g}{\partial c^4}\bigg|_{\bar{\phi},\bar{c},\bar{s}} \delta c^4 + \frac{1}{4!}\frac{\partial^4 g}{\partial s^4}\bigg|_{\bar{\phi},\bar{c},\bar{s}} \delta s^4$$

$$+ C|\nabla\phi|^2 + \left[\rho\Phi - \frac{1}{8\pi l_B}|\nabla\Phi|^2\right] \qquad (18)$$

where

$$g(\phi,c,s) = \frac{\zeta}{6}\times\frac{\phi}{2}\left(2+\left(\frac{\overline{\phi}}{\phi}\right)^2\right)-\frac{\phi}{3}\ln\left[1-\frac{\zeta}{2}\left(2+\left(\frac{\overline{\phi}}{\phi}\right)^2\right)\right] + \chi\phi(1-\phi)+(1-\phi)\ln(1-\phi)+c\ln c+s\ln s \quad (19)$$

The linear and cubic order terms in eq 18 vanish due to the symmetry of lamellar phases. However, for more general deformations, a cubic term retains for patterns such as hexagonal and body-centered cubic phases, and it plays a crucial role in phase competition.

In the limit that the variations $\{\delta\phi, \delta c, \delta s\}$ are small, these variations of periodic lamellar phases (with periodicity of $2\pi/k$) can be approximated as plane waves with the wavenumber k, that is

$$\delta\phi = A_\phi(e^{ikx}+e^{-ikx}),\quad \delta c = A_c(e^{ikx}+e^{-ikx}),\quad \delta s = A_s(e^{ikx}+e^{-ikx}) \quad (20)$$

where A_ϕ, A_c, and A_s are the corresponding amplitudes. In contrast to the case of neutral polymer blends where the minority component varies as the second harmonic $2k$,[33] the co-ions and counterions in the charged gel adapt the same principal wavenumber due to electrostatic interactions. Note that the plane wave approximation is only valid when the thermal fluctuations are much smaller than the density variations. For an isotropic system, it is well established that including fluctuations could dramatically change the transition phase boundary as well as the stability of competing patterns.[34−39]

The free energy can be expressed in terms of these amplitudes and k by substituting above ansatz eq 20 into eq 18. For example, the gradient energy and electrostatic energy are given as,

$$\int \mathrm{d}\vec{r}\; C|\nabla\phi|^2 = \int \mathrm{d}\vec{r}\; 4Ck^2A_\phi{}^2\sin^2 kx \quad (21)$$

and

$$\int\left[\rho\Phi-\frac{1}{8\pi l_B}|\nabla\Phi|^2\right]\mathrm{d}\vec{r} = \int\frac{1}{2}\rho\Phi\,\mathrm{d}\vec{r} = \int 8\pi l_B\frac{(A_s-A_c-fA_\phi)^2}{k^2}\cos^2 kx\,\mathrm{d}\vec{r} \quad (22)$$

After integrating over one periodicity, eq 18 is reduced to a function of $\{A_\phi,A_c,A_s\}$ and k. The solutions of $\{A_\phi,A_c,A_s\}$ and k are obtained by requiring that the derivatives of the free energy with respect to each of these variables vanish (i.e., $\partial\mathscr{F}/\partial A_\phi = 0$, $\partial\mathscr{F}/\partial A_c = 0$, $\partial\mathscr{F}/\partial A_s = 0$ and $\partial\mathscr{F}/\partial k = 0$). The free energy is then calculated by substituting these solutions into the free energy expression. We define the excess free energy density as

$$\Delta\mathscr{F} = \frac{k}{2\pi}(\mathscr{F}-\int g(\overline{\phi},\overline{c},\overline{s})\,\mathrm{d}\vec{r}) \quad (23)$$

Nanophase segregation is favored when $\Delta\mathscr{F} < 0$ and the solution exists for a finite value of k.

Figure 6 shows the solutions of $\{A_\phi, A_c, A_s\}$ as functions of the salt concentration c_s. The absolute value of amplitudes grows with salt concentration; and the amplitude of co-ions has opposite sign with respect to that of polymer and counterions as a result of electrostatic repulsion.Figure 7 shows the solution of k as a function of the salt concentration c_s, compared against numerical solutions of eq 6. The prediction of wavenumber from weakly nonlinear analysis is in good agreement with numerical

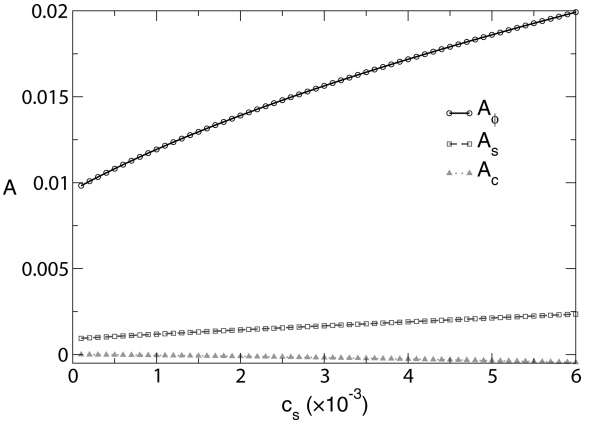

Figure 6. Solutions of amplitudes from weakly nonlinear analysis as functions of salt concentration. The model parameters are $\bar{\phi} = 0.05$, $N = 100$, $\chi = 2.4$, $f = 0.5$, and $l_B = 1$.

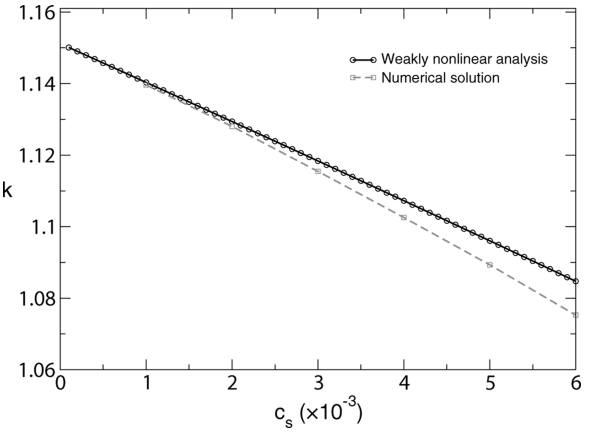

Figure 7. Comparison of wavenumber obtained from the weakly nonlinear analysis and the numerical solution. The model parameters are $\bar{\phi} = 0.05$, $N = 100$, $\chi = 2.4$, $f = 0.5$, and $l_B = 1$. The discrepancy between weakly nonlinear analysis and the numerical solution is less than 1% at $\bar{c} = 6\times10^{-3}$.

solutions at low salt concentration. As the salt concentration increases, the predictions of weakly nonlinear analysis deviates from numerical solutions since the assumption of small perturbations around the mean value is no longer valid. The comparison of volume fraction profiles obtained by the weakly nonlinear analysis and the numerical solutions are shown in Figure 8. Again, the weakly nonlinear analysis accurately describes the lamellar nanophases in the low salt regime, see Figure 8a. Figure 8b gives an example of volume fraction profiles near the critical salt concentration, where macrophase separation is expected to occur if more salts are added, and the weakly nonlinear analysis begins to deviate from the numerical solution.

It is interesting to note that the length scale of the nanophase arises from the competition between energy contributed from inhomogeneities and the electrostatic energy, since all other terms do not depend on k explicitly. The relation between the wavenumber and amplitudes is determined by the equation,

$$\frac{\partial\mathscr{F}}{\partial k} = 0 = 4CkA_\phi^2-\frac{8\pi l_B}{k^3}(A_s-A_c-fA_\phi)^2 \quad (24)$$

which results in

$$k = \left(\frac{2\pi l_B(A_s-A_c-fA_\phi)^2}{CA_\phi{}^2}\right)^{1/4} \quad (25)$$

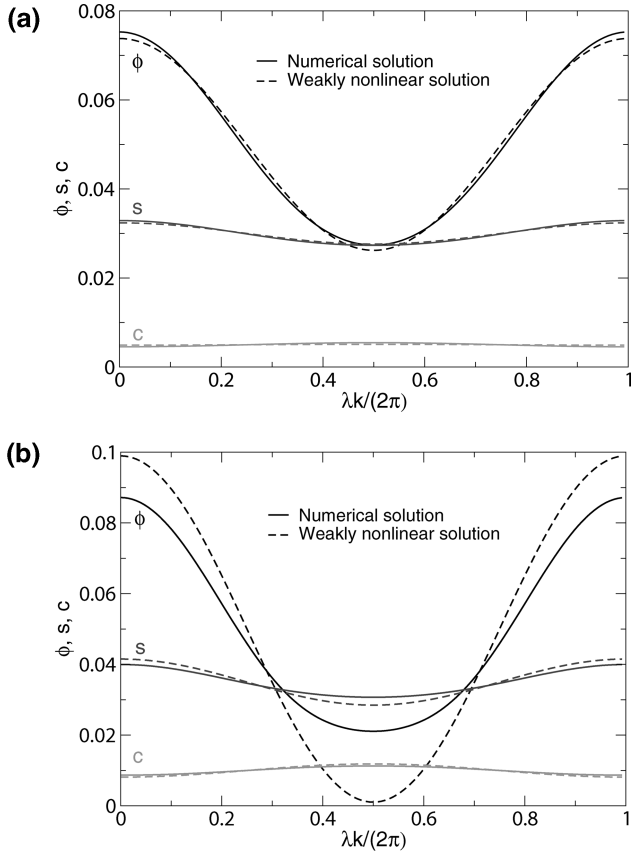

Figure 8. Comparison of equilibrium distribution of volume fractions obtained from weakly nonlinear analysis and the numerical solution. The model parameters are $\bar{\phi} = 0.05$, $N = 100$, $\chi = 2.4$, $f = 0.5$, and $l_B = 1$. The salt concentration is $\bar{c} = 5 \times 10^{-3}$ and $\bar{c} = 1 \times 10^{-2}$ in parts a and b, respectively.

The salt effect on the volume fraction of polymer gels can be derived using eq 23. We have

$$\Delta\mathcal{F} = \Delta\mathcal{F}_\phi(A_\phi) + 2Ck^2{A_\phi}^2 + \frac{4\pi l_B}{k^2}(A_s - A_c - fA_\phi)^2 + \frac{1}{\bar{c}}{A_c}^2 + \frac{1}{2\bar{c}^3}{A_c}^4 + \frac{1}{\bar{s}}{A_s}^2 + \frac{1}{2\bar{s}^3}{A_s}^4 \quad (26)$$

where

$$\Delta\mathcal{F}_\phi(A_\phi) \equiv -2\chi{A_\phi}^2 - \frac{1}{\bar{\phi}-1}{A_\phi}^2 + \frac{1}{2(\bar{\phi}-1)^3}{A_\phi}^4 + \frac{1}{\bar{\phi}}\left(\frac{4}{3}\beta^2 - \frac{2}{3}\beta\right){A_\phi}^2 + \frac{\zeta}{6\bar{\phi}}{A_\phi}^2 + \frac{\zeta}{2\bar{\phi}^3}{A_\phi}^4 + \frac{1}{\bar{\phi}^3}\left(8\beta^4 - \frac{56}{3}\beta^3 + 13\beta^2 - 2\beta\right){A_\phi}^4 \quad (27)$$

and $\beta \equiv \zeta/(3\zeta - 2)$. The condition that A_c minimizes the free energy gives rise to

$$\frac{\partial\Delta\mathcal{F}}{\partial A_c} = 0 = \frac{2}{\bar{c}}A_c + \frac{2}{\bar{c}^3}{A_c}^3 - \frac{8\pi l_B}{k^2}(A_s - A_c - fA_\phi) \quad (28)$$

Substituting k using eq 25 in the above equation, we obtain

$$\frac{2}{\bar{c}}A_c + \frac{2}{\bar{c}^3}{A_c}^3 + 4(2\pi l_B C)^{1/2}A_\phi = 0 \quad (29)$$

In the limit that $A_c/\bar{c} \ll 1$, we have

$$A_c = -\bar{c}\sqrt{8\pi l_B C}A_\phi \quad (30)$$

which has the opposite sign to A_ϕ, consistent with the results in Figure 6. Repeating the same calculation for A_s, we obtain

$$A_s = \bar{s}\sqrt{8\pi l_B C}A_\phi \quad (31)$$

The dependence of the characteristic length scale of the nanophase on salt concentration is obtained by substituting eq 30 and eq 31 into eq 25, we obtain

$$k = \left(\frac{2\pi l_B}{C}\right)^{1/4}(f - (2\bar{c} + f\bar{\phi})\sqrt{8\pi l_B C})^{1/2} \quad (32)$$

Hence, the wavenumber of the nanophase decreases as the salt concentration increases as shown in Figure 7. The salt dependence of A_ϕ can be derived using $\partial\Delta\mathcal{F}/\partial A_\phi = 0$, which yields

$$\frac{\partial\Delta\mathcal{F}}{\partial A_\phi} = \Delta'\mathcal{F}_\phi(A_\phi) + 4Ck^2A_\phi - \frac{8\pi l_B f}{k^2}(A_c - A_s - fA_\phi) = 0 \quad (33)$$

where $\Delta'\mathcal{F}_\phi(A_\phi)$ is the derivative of $\Delta\mathcal{F}_\phi$ with respect to A_ϕ, and has a general form $\Delta'\mathcal{F}_\phi(\mathrm{A}_\phi) = \alpha_1 A_\phi + \alpha_3 {A_\phi}^3$. Using eqs 25, 30, and 31; eq 33 reduces to

$$\frac{\partial\Delta\mathcal{F}}{\partial A_\phi} = \Delta'\mathcal{F}_\phi(A_\phi) + 2\sqrt{8\pi l_B C}(2f - (2\bar{c} + f\bar{\phi})\sqrt{8\pi l_B C}) = \alpha'_1 A_\phi + \alpha_3 A_\phi^3 = 0 \quad (34)$$

where

$$\alpha'_1 \equiv \alpha_1 + 2\sqrt{8\pi l_B C}(2f - (2\bar{c} + f\bar{\phi})\sqrt{8\pi l_B C}) \quad (35)$$

and the amplitude is

$$A_\phi = \left(-\frac{\alpha'_1}{\alpha_3}\right)^{1/2} \quad (36)$$

Since α_3 is positive, it requires that $\alpha'_1 < 0$ in order to have nanophases. In this regime, as salt concentration increases, α'_1 becomes more negative; thus, A_ϕ becomes larger that is consistent with results shown in Figure 6. In addition, the above analysis elucidates the role of salt controlling transition from swollen gels to nanophases. When α'_1 is greater than zero, the solution of A_ϕ is zero that corresponds to a swollen gel. The transition from swollen gels to lamellar nanophases occurs as α'_1 changes sign as salt concentration increases. The phase boundaries between swollen gel and nanophase computed using the weakly nonlinear analysis with the condition that $\alpha'_1 = 0$ are compared to numerical solutions in Figure 4 and Figure 5. The weakly nonlinear predictions are in quantitatively good agreement with numerical solutions.

It is important to note that effects of thermal fluctuations can be included in the above analysis using Hartree approximation,[34−38] wherein the total free energy is a sum of the mean field free energy and the Hartree contribution. When fluctuations for different wave vectors are uncorrelated, the Hartree contribution contains solely a quadratic term that modifies the quadratic coefficient α'_1 which leads to a shift of the phase boundary.

Conclusions

We have presented a continuum theory of polyelectrolyte gels that includes van der Waals forces, entropy of mobile ions, elasticity of the network structure, interfacial energy due to

polymer inhomogeneities, and Coulomb interactions. The numerical solutions show that the nanophases can be induced from a swollen gel by the addition of salt, and a complete collapse occurs as the salt concentration exceeds a critical value for gels in poor solvent. The transition from the homogeneous phase to a strongly correlated periodic state is expected to be first order in nature. We show that the wavelength of nanophases can be controlled by varying salt concentration which suggests a possible means to design nanostructures. In addition, we show that the phase diagrams of polyelectrolyte gels are significantly affected by the Bjerrum length that relates to the dielectric permittivity of solvent, and hence provide an additional means of control. The nanophases are shown to be favored for high solvent permittivity and/or low salt concentrations. We have also derived a weakly nonlinear analysis of polyelectrolyte gels to predict the swollen gel−nanophase transition so as to provide extra insight into the salt effects we observe in the numerical solutions. Since the weakly nonlinear analysis reasonably predicts the volume fractions profiles and the wavelength of nanophases, it is useful as a guide to estimate these values without having to solve the full nonlinear problem. However, we expect fluctuations to modify these predictions if the transition is predicted to be nearly continuous. Moreover, we expect the weakly nonlinear analysis to fail near macrophase separation transition since the small variation assumption of volume fractions is no longer valid. Thermal fluctuations can be included in the current approach by adding a stochastic noise term in the evolution equations.[40]

In the present work, we limit our analysis to salt effects in uniformly cross-linked gels. This ideal scenario is hard to achieve in experiments, that are further complicated by the effects of cross-link inhomogeneities, which in turn depends on the conditions of preparation.[41−43] Also, while the existence of a characteristic wavelength in the nanometer range is clearly demonstrated in scattering experiments on PE gels in poor solvent conditions,[14,18,21] we are not aware of an experimental evidence of the periodic symmetry of nanostructures. This might be due to the presence of thermal fluctuations that are expected to suppress the periodicity of the nanostructures, and may lead to the formation of percolated structures,[44] or deformed lamellar structures with no long-range periodicity. Nevertheless, we believe, well-defined periodic structures can be realized in controlled experimental systems containing PE gels where electrostatic interactions are dominant, similar to the lamellar nanostructures observed in recent studies on polyelectrolyte-diblock copolymer gels.[45] Further, we only consider monovalent salt in this study since our model does not resolve short-range electrostatic correlation effects (e.g., ion condensation and ion pairing) observed in multivalent salt solutions.[46−51] The treatment of short-range electrostatic correlations is problematic within this continuum approach, as opposed to particle-based simulation methods.[52−56] Unfortunately, the advantages of particle-based simulation methods are overshadowed by the limitations on the simulation size that can be studied, because of the large relaxation times of polymer network and expensive computation of long-range interactions.

Our methodology provides a useful guide to design and engineer nanophases in polyelectrolyte gels. Although we consider only lamellar nanostructures in this paper, other structures can be obtained by the same formulation with a more general deformation of gels. The weakly nonlinear analysis can also be easily generalized to general deformations. It is of interest to use this method to investigate stability of different phases to obtain a complete phase diagram and study phase transition between different phases. In addition, a time-dependent Ginzburg−Landau approach is used to obtain the steady state solution of resulting free energy. Although the time evolution of gels is irrelevant in this study, this approach can be used to study the dynamic phenomenon in gels associated with the gelation process[57−59] chemical reactions.[60−62] Further, for simplicity in consideration, we limited our model to strongly charged gels with a fixed charge fractions at a constant pH and constant dielectric permittivity. However, an extension of this idea to include the effects of charge regulation brought by changes in pH,[63,64] or an interfacial adsorption due to dielectric inhomogeneities[65−67] is straightforward. Efforts in these directions are currently underway.

Acknowledgment. The authors thank Francisco Solis and Jos Zwanikken for stimulating discussions. P.K.J. is supported by NSF under Award No. DMR-0907781. M.O.d.l.C. is grateful for a National Security Science and Engineering Faculty Fellowship (NSSEFF) from the U.S. Department of Defense.

Note Added after ASAP Publication. This paper was published on the Web on October 4, 2010, with an erroneous definition of greek zeta (ζ) below equation 4. The corrected version was reposted on October 6, 2010.

References and Notes

(1) Qiu, Y.; Park, K. *Adv. Drug Deliver. Rev.* **2001**, *53*, 321–339.
(2) Lendlein, A.; Kratz, K.; Kelch, S. *Med. Device Tech.* **2005**, 12–15.
(3) Malmsten, M. *Soft Matter* **2006**, *2*, 760–69.
(4) Ahn, S.; Kasi, R. M.; Kim, S.; Sharma, N.; Zhou, Y. *Soft Matter* **2008**, *4*, 1151–57.
(5) He, C.; Kim, S. W.; Lee, D. S. *J. Controlled Release* **2008**, *127*, 189–207.
(6) Calvert, P. *Adv. Mater.* **2009**, *21*, 743–756.
(7) Tanaka, T.; Fillmore, D.; Sun, S.-T.; Nishio, I.; Swislow, G.; Shah, A. *Phys. Rev. Lett.* **1980**, *45*, 1636–1639.
(8) Tanaka, T.; Nishio, I.; Sun, S.-T.; Ueno-Nishio, S. *Science* **1982**, *218*, 467–469.
(9) Tanaka, T.; Sun, S.-T.; Hirokawa, Y.; Katayama, S.; Kuccera, J.; Hirose, Y.; Amiya, T. *Nature* **1987**, *325*, 796–798.
(10) Tanaka, T.; Annaka, M. *J. Intelligent Mater. Sys.* **1993**, *4*, 548–552.
(11) Dobrynin, A. V. *Curr. Opin. Colloid Interface Sci.* **2008**, *13*, 376–388.
(12) Hong, W.; Zhao, X.; Suo, Z. *J. Mech. Phys. Solids* **2010**, *58*, 558–577.
(13) Schosseler, F.; Ilmain, F.; Candau, S. J. *Macromolecules* **1991**, *24*, 225.
(14) Shibayama, M.; Tanaka, T.; Han, C. *J. Chem. Phys.* **1992**, *97*, 6829.
(15) Shibayama, M.; Tanaka, T.; Han, C. *J. Chem. Phys.* **1992**, *97*, 6842.
(16) Kramarenko, E. Y.; Khokhlov, A. R. *Polym. Gels Networks* **1998**, *6*, 45–56.
(17) Shibayama, M. In *Structure and Properties of Multiphase Polymeric Materials*; Marcel Dekker Inc.: New York, 1998; pp 195−232.
(18) Ikkai, F.; Suzuki, T.; Karino, T.; Shibayama, M. *Macromolecules* **2007**, *40*, 1140–1146.
(19) Ikkai, F.; Shibayama, M. *Polymer* **2007**, *48*, 2387–2394.
(20) Bastide, J.; Mendes, E.; Boue, F.; Buzier, M.; Lindner, P. *Makromol. Chem.—Mol. Symp.* **1990**, *40*, 81.
(21) Shibayama, M. *Macromol. Chem. Phys.* **1998**, *199*, 1–30.
(22) Ikkai, F.; Shibayama, M. *J. Polym. Sci., Part B* **2005**, *43*, 617–628.
(23) Flory, P. J. *Principles of polymer chemistry*; Cornell University Press: New York, 1953.
(24) Onuki, A. *Phase Transitions Dynamics*; Cambridge University Press: Cambridge, U.K., 2002.
(25) Mark, J. E.; Erman, B. *Rubberlike Elasticity: A Molecular Primer*; Cambridge University Press: Cambridge, U.K., 2007.
(26) Donnan, P. G.; Guggenheim, E. A. *Z. Phys. Chem.* **1934**, *162*, 364.
(27) Panyukov, S.; Rabin, Y. *Macromolecules* **1996**, *29*, 8530–8537.
(28) Rabin, Y.; Panyukov, S. *Macromolecules* **1997**, *30*, 301–312.
(29) Zeldovich, K. B.; Dormidontova, E. E.; Khokhlov, A. R.; Vilgis, T. A. *J. Phys. II France* **1997**, *7*, 627–635.
(30) Jha, P. K.; Solis, F. J.; de Pablo, J. J.; de la Cruz, M. O. *Macromolecules* **2009**, *42*, 6284–6289.
(31) Hesthaven, J.; , S. G.; Gottlieb, D. *Spectral methods for time-dependent problems*; Cambridge University Press: Cambridge, U.K., 2007.
(32) Slater, G. W.; Gratton, Y.; Kenward, M.; McCormick, L.; Tessier, F. *Soft Mater.* **2004**, *2*, 155–182.

(33) Huang, C.; de la Cruz, M. O. *Phys. Rev. E* **1996**, *53*, 812–819.
(34) Brazovskii, A. *JETP* **1975**, *41*, 85.
(35) Fredrickson, G. H.; Helfand, E. *J. Chem. Phys.* **1987**, *87*, 697–705.
(36) de la Cruz, M. O. *Phys. Rev. Lett.* **1991**, *67*, 85–88.
(37) Melenkevitz, J.; Muthukumar, M. *Macromolecules* **1991**, *24*, 4199–4205.
(38) Jones, J. L.; de la Cruz, M. O. *J. Chem. Phys.* **1994**, *100*, 5272–5279.
(39) Ciach, A.; Góźdź, W. T.; Stell, G. *Phys. Rev. E 75*, 051505, 2007.
(40) Hohenberg, P. C.; Halperin, B. I. *Rev. Mod. Phys.* **1977**, *49*, 435–479.
(41) Shibayama, M.; Ikkai, F.; Shiwa, Y.; Rabin, Y. *J. Chem. Phys.* **1997**, *107*, 5227–5235.
(42) Ikkai, F.; Shibayama, M.; Han, C. C. *Macromolecules* **1998**, *31*, 3275–3281.
(43) Ikkai, F.; Iritani, O.; Shibayama, M.; Han, C. C. *Macromolecules* **1998**, *31*, 8526–8530.
(44) Yin, D.-W.; de la Cruz, M. O.; de Pablo, J. J. *J. Chem. Phys.* **2009**, *131*, 194907.
(45) Kang, Y.; Walish, J. J.; Gorishnyy, T.; Thomas, E. L. *Nat. Mater.* **2007**, *6*, 957–960.
(46) de la Cruz, M. O.; Belloni, L.; Delsanti, M.; Dalbiez, J. P.; Spalla, O.; Drifford, M. *J. Chem. Phys.* **1995**, *103*, 5781.
(47) Dobrynin, A. V.; Rubinstein, M. *Macromolecules* **1996**, *29*, 2974–2979.
(48) Solis, F. J.; de la Cruz, M. O. *J. Chem. Phys.* **2000**, *112*, 2030.
(49) Liao, Q.; Dobrynin, A. V.; Rubinstein, M. *Macromolecules* **2003**, *36*, 3399–3410.
(50) Hutchens, S. B.; Wang, Z.-G. *J. Chem. Phys.* **2007**, *127*, 084912.
(51) de la Cruz, M. O. *Soft Matter* **2008**, *4*, 1735–1739.
(52) Yan, Q.; de Pablo, J. J. *Phys. Rev. Lett.* **2003**, *91*, 018301.
(53) Yin, D.-W.; Yan, Q.; de Pablo, J. J. *J. Chem. Phys.* **2005**, *123*, 174909.
(54) Mann, B. A.; Kremer, K.; Holm, C. *Mol. Simul.* **2006**, *237*, 90–107.
(55) Edgecombe, S.; Linse, P. *Macromolecules* **2007**, *40*, 3868–3875.
(56) Yin, D. W.; Horkay, F.; Douglas, J. F.; de Pablo, J. J. *J. Chem. Phys.* **2008**, *129*, 154902.
(57) Ermoshkin, A. V.; de la Cruz, M. O. *Phys. Rev. Lett.* **2003**, *90*, 125504.
(58) Guo, L.; Luijten, E. *J. Polym. Sci., Part B* **2005**, *43*, 959–969.
(59) de la Cruz, M. O.; Ermoshkin, A. V.; Carignano, M. A.; Szleifer, I. *Soft Matter* **2009**, *5*, 629–636.
(60) Campbell, C. J.; Klajn, R.; Fialkowski, M.; Grzybowski, B. A. *Langmuir* **2005**, *21*, 418–423.
(61) Nakanishi, H.; Satoh, M.; Norisuye, T.; Tran-Cong-Miyata, Q. *Macromolecules* **2004**, *37*, 8495–8498.
(62) Yashin, V. V.; Balazs, A. C. *Science* **2006**, *314*, 798–801.
(63) Plotnikov, N.; Victorov, A. *Fluid Phase Equilib.* **2007**, *261*, 26–34.
(64) Tagliazucchi, M.; de la Cruz, M. O.; Szleifer, I. *Proc. Natl. Acad. Sci. U.S.A.* **2010**, *107*, 5300–5305.
(65) Dzubiella, J.; Swanson, J. M. J.; McCammon, J. A. *Phys. Rev. Lett.* **2006**, *96*, 087802.
(66) Kung, W.; Solis, F. J.; de la Cruz, M. O. *J. Chem. Phys.* **2009**, *130*, 044502.
(67) Bier, M.; de Graaf, J.; Zwanikken, J.; van Roij, R. *J. Chem. Phys.* **2009**, *130*, 024703.